Heavy Quasiparticles in the Ferromagnetic Superconductor $ZrZn_2$

S. J. C. Yates, G. Santi, S. M. Hayden, P. J. Meeson, and S. B. Dugdale
H. H. Wills Physics Laboratory, University of Bristol, Tyndall Avenue, Bristol BS8 1TL, United Kingdom
(Received 10 July 2002; published 6 February 2003)

We report a study of the de Haas–van Alphen effect in the normal state of the ferromagnetic superconductor $ZrZn_2$. Our results are generally consistent with a linear muffin-tin orbital band structure which predicts four exchange-split Fermi surface sheets. Quasiparticle effective masses are enhanced by a factor of 4.9 implying a strong coupling to magnetic excitations or phonons. $ZrZn_2$ is unique among metallic ferromagnets in that it has a very large density of states in the ferromagnetic phase.

DOI: 10.1103/PhysRevLett.90.057003 PACS numbers: 74.70.Ad, 71.18.+y, 74.25.Jb

The recent reports of the coexistence of ferromagnetism and superconductivity in UGe_2 [1], $ZrZn_2$ [2], URhGe [3] as well as the discovery of superconductivity in the nonmagnetic hcp phase of Fe under pressure [4] have reopened the debate regarding the relationship of magnetism and superconductivity. Motivated by the case of liquid ^{3}He, the search for superconductivity mediated by spin fluctuations in nearly magnetic materials has a long history [5]. The observation of superconductivity in the ferromagnetic phase of $ZrZn_2$ [2] (as well as UGe_2 and URhGe), together with the extreme sensitivity of its occurrence to sample purity [2,6], makes it a strong candidate for magnetically mediated spin-triplet superconductivity, as is believed to exist in Sr_2RuO_4 [6,7], although other scenarios are not excluded [8]. A detailed knowledge of the electronic structure of $ZrZn_2$ is crucial to the understanding of both its normal and superconducting properties. Thus we report here a detailed study of the Fermi surface (FS) made using angle-resolved measurements of the de Haas–van Alphen effect (dHvA). Our results are compared with an *ab initio* electronic structure calculation.

$ZrZn_2$ orders ferromagnetically at $T_{\mathrm{FM}} \simeq 28$ K, with an ordered moment of $0.17\mu_B$ per formula unit at $T = 2$ K. The intrinsic moment is unsaturated, with a field of 6 T causing a 50% increase. Compared with other d-band metals, it has an extremely large electronic heat capacity at low temperatures of $C/T = 47\ \mathrm{mJ\,K^{-2}\,mol^{-1}}$. $ZrZn_2$ crystallizes in the C15 cubic Laves structure, with lattice constant $a = 7.393$ Å, the Zr atoms forming a tetrahedrally coordinated diamond structure. Its magnetic properties derive from the Zr $4d$ orbitals, which have a significant direct overlap.

Interest in $ZrZn_2$ has been rekindled by the discovery that it is superconducting at ambient pressure and that both the superconductivity and ferromagnetism are simultaneously destroyed by the application of hydrostatic pressure. For the samples considered here, the onset temperature for the superconductivity is $T_{\mathrm{SC}} \approx 0.6$ K with $B_{c2} \approx 0.9$ T. The most striking feature of $ZrZn_2$, UGe_2, and URhGe is perhaps that the *same* electrons are thought to participate both in superconductivity and ferromagnetism, in contrast with other "magnetic" superconductors, e.g., borocarbides, $RuSr_2GdCu_2O_8$ [9], where the magnetism and superconductivity occur in different parts of the unit cell. Furthermore, $ZrZn_2$ is a 3D intermetallic compound in which the itineracy of the d electrons is almost unquestionable, whereas some doubts remain about that of the $5f$ electrons and the roles of the strong magnetocrystalline anisotropy and quasi-2D electronic structure in UGe_2 and URhGe.

The dHvA effect is due to the quantization of the cyclotron motion of charge carriers and results in a magnetization, M_{osc}, which oscillates with magnetic field, $\mathbf{B}$. We interpret our results using the Lifshitz-Kosevich expression [10] in which each extremal area A of a FS sheet perpendicular to $\hat{\mathbf{B}}$ gives a contribution to the oscillatory magnetization,

$$M_{\mathrm{osc}} \propto B^{1/2} R_D R_T \sin\left(\frac{2\pi F}{B} + \gamma\right), \tag{1}$$

where $F(\hat{\mathbf{B}}) = (\hbar/2\pi e)A(\hat{\mathbf{B}})$. R_D and R_T are the Dingle and temperature damping factors, respectively. The temperature dependence of M_{osc} yields the cyclotron mass, m^*, through $R_T = X/\sinh X$ where $X = 2\pi^2 k_B T m^*/(\hbar e B)$. This mass includes all many-body renormalizations and is related to the corresponding orbit through

$$m^* = \frac{\hbar}{2\pi} \oint_{\mathrm{FS\ orbit}} \frac{dk}{v_F}. \tag{2}$$

The quasiparticle lifetime, τ, and the mean-free path, l, can be determined on each orbit via the field-dependent factor $R_D = \exp(-\pi m_b/eB\tau)$. Equation (1) has no "spin-splitting factor" [10] since in a ferromagnet, spin-split sheets of the FS are resolved separately.

The dHvA magnetization was measured using a standard low-frequency field-modulation technique. Data were collected using a top-loading dilution refrigerator equipped with a 13.5 T magnet reaching temperatures as low as 30 mK and with a ^{3}He system equipped with an

 0031-9007/03/90(5)/057003(4)$20.00

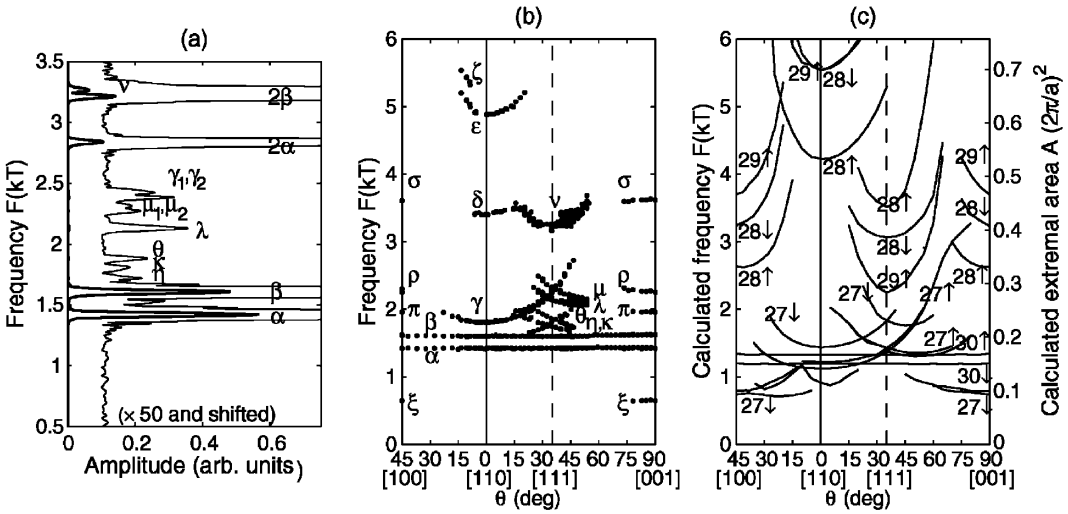

FIG. 1. (a) A dHvA spectrum collected for **B** applied 1.5° from [111] towards [001]. Data were collected in the range $7 < B < 13.4$ T at $T = 25$ mK. (b) The angular dependence of the dHvA frequencies. (c) Calculated dHvA frequencies.

18 T magnet. High-quality samples ($\rho_0 = 0.6\ \mu\Omega$ cm) were prepared by directional cooling of a $ZrZn_2$ melt contained in an Y_2O_3 crucible inside a tantalum bomb [2].

We performed angle-resolved dHvA measurements for fields applied perpendicular to the [001] and [1$\bar{1}$0] directions. Figure 1(a) shows a typical Fourier transform of our dHvA data collected for $\hat{\mathbf{B}}$ close to [111]. The spectrum is dominated by the low frequencies $F_\alpha = 1.42$ kT and $F_\beta = 1.60$ kT and their harmonics. These have been previously assigned to an exchange-split pocket of the FS centered on the Γ point of the Brillouin zone [see Fig. 2(a)]. The frequency difference $F_\alpha - F_\beta$ measures the ferromagnetic exchange splitting. In addition to α and β, we also observe a number of closely spaced frequencies in the range 1.6–2.5 kT (η, κ, θ, λ, μ, and γ) and a strong component ν near 3.2 kT. Some frequency branches (μ and γ) appear as multiplets. In all, our study revealed 17 frequency branches, whose angular dependences are shown in Fig. 1(b). Branches α, β, and ν were observed in previous studies [11] and are in good agreement with our work. In addition to extremal FS areas, the temperature dependence of the dHvA amplitude enables the determination of the cyclotron effective mass corresponding to each orbit (see Table I) from the factor R_T in Eq. (1).

To understand our results, we performed self-consistent spin-polarized band structure calculations using the linear muffin-tin orbital method within the local-spin-density approximation (LSDA) [12]. We obtained a relaxed lattice constant, $a = 7.223$ Å and a magnetic moment, $\mu = 0.18\mu_B/\mathrm{Zr}$ in agreement with the measured one (of $0.17\mu_B/\mathrm{Zr}$ [2]). Our calculation agrees well with others [8,13]. The resulting FS and density of states (DOS) are shown in Fig. 2. The angular dependence of the dHvA frequencies [see Fig. 1(c)] imposes strong constraints on the possible topologies of the FS and

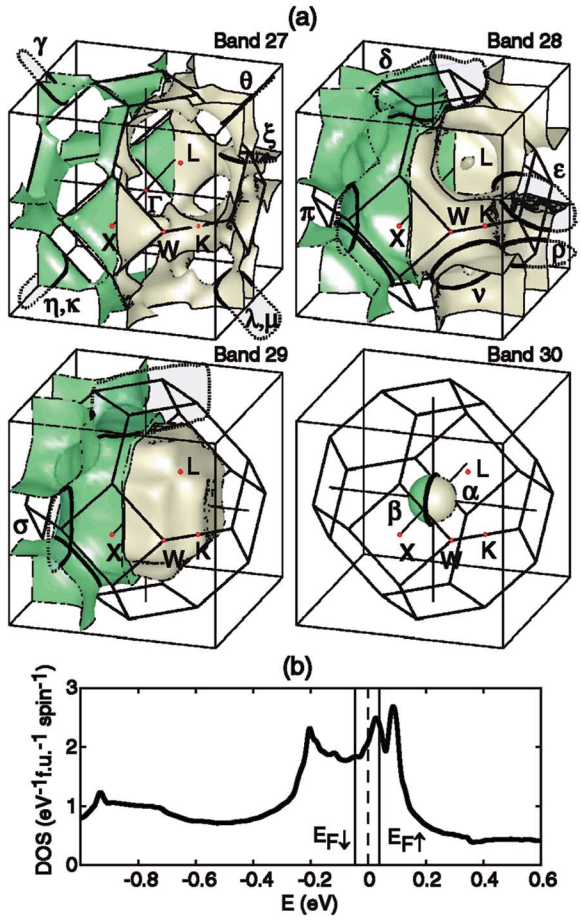

FIG. 2 (color online). (a) Calculated Fermi surface of $ZrZn_2$ for the four bands crossing E_F. The left and right parts of each figure are the majority (↑) and minority (↓) spin sheets, respectively. Labeled solid lines are some of the orbits discussed in the text. (b) The calculated DOS for paramagnetic $ZrZn_2$ (see text). The vertical solid lines represent the energy shift of the spin ↑ and ↓ Fermi energies in the ferromagnetic state.

TABLE I. Experimental and calculated dHvA frequencies and cyclotron masses for $\langle B \rangle = 9.2$ T. Branch assignments refer to Fig. 1(b) and the FS orbits are denoted by orbit center, band index, and spin ($\uparrow$ is majority).

Experiment			Calculation			
Branch	F (kT)	m^* (m_e)	FS Orbit		F (kT)	$\lvert m_b \rvert$ (m_e)
			B ∥ [110]			
α	1.425	0.81(4)	$\Gamma_{30,\downarrow}$	(sphere)	1.193	0.24
β	1.600	0.95(5)	$\Gamma_{30,\uparrow}$	(sphere)	1.329	0.26
γ	1.810	1.27(3)	$X_{27,\downarrow}$	(pillow)	1.438	0.51
δ	3.400	3.7(10)	$X_{28,\uparrow}$	(dog bone)	4.227	2.19
ϵ	4.770	3.9(2)	$X_{28,\downarrow}$	(dog bone)	5.538	1.53
ζ	5.300	3.5(10)				
			$X_{29,\uparrow}$	(dog bone)	5.541	4.25
			$\Gamma_{29,\downarrow}$	(belly)	12.466	4.02
			B ∥ [111]			
α	1.425	0.82(5)	$\Gamma_{30,\downarrow}$	(sphere)	1.193	0.24
β	1.600	1.00(4)	$\Gamma_{30,\uparrow}$	(sphere)	1.328	0.26
η	1.740	3(1)	$X_{27,\uparrow}$	(pillow)	1.432	1.16
θ	1.809	2(1)	$X_{27,\uparrow}$	(pillow)	1.376	0.64
κ	1.860	3(2)	$X_{27,\uparrow}$	(pillow)	1.376	0.64
λ_1	2.140	1.6(1)	$X_{27,\downarrow}$	(pillow)	1.833	0.76
λ_2	2.180		$X_{27,\downarrow}$	(pillow)		
γ_1	2.240	1.9(1)	$X_{27,\downarrow}$	(pillow)	1.833	0.76
γ_2	2.272	3.1(2)	$X_{27,\downarrow}$	(pillow)		
μ_1	2.307	1.4(3)	$X_{27,\downarrow}$	(pillow)	1.833	0.76
μ_2	2.330	2.4(4)	$X_{27,\downarrow}$	(pillow)		
ν_1	3.170	2.20(6)		(neck)		
ν_2	3.230	1.60(3)	$L_{28,\downarrow}$	(neck)	3.067	0.53
ν_3	3.260	1.45(5)		(neck)		
			$L_{29,\uparrow}$	(neck)	2.250	7.89
			$L_{28,\uparrow}$	(neck)	3.517	1.33
			$\Gamma_{29,\downarrow}$	(belly)	12.766	4.76
			B ∥ [001]			
ξ	0.645	4(2)	$W_{27,\downarrow}$	(pillow neck)	0.767	0.68
α	1.420	0.9(1)	$\Gamma_{30,\downarrow}$	(sphere)	1.201	0.24
β	1.610	1.1(1)	$\Gamma_{30,\uparrow}$	(sphere)	1.340	0.26
π	1.970	4(1)	$W_{28,\uparrow}$	(rosette)	2.626	1.28
ρ	2.270	7(2)	$W_{28,\downarrow}$	(rosette)	3.232	0.94
σ	3.630	5(2)	$W_{29,\uparrow}$	(rosette)	3.699	7.96
			$\Gamma_{29,\downarrow}$	(belly)	11.699	3.51
			$\Gamma_{28,\downarrow}$	(belly)	13.335	3.05
			$\Gamma_{29,\uparrow}$	(belly)	14.228	4.03
			$\Gamma_{28,\uparrow}$	(belly)	15.894	4.30

therefore allows the validity of the calculated FS to be verified. The cyclotron band mass for each extremal orbit (see Table I) is obtained from $m_b = (\hbar^2/2\pi)(\partial A/\partial E)_{E_F}$ by numerical differentiation with $\Delta E = 0.5$ mRy.

The *ab initio* calculated FS reproduces the essential topology of the observed one. We assign α and β to the spin-split spherical FS sheet Γ_{30} as in previous studies [11]. The complex of branches observed near [111] including γ, η, θ, κ, λ, and μ appears to be due to orbits associated with the X-centered "pillow" features of band 27. Both spin $\uparrow$ and $\downarrow$ FS sheets show this feature; thus there are pairs of exchange-split branches such as θ and γ and (η, κ) and (λ, μ). The θ branch is probably obscured by the strong α branch near [110], only allowing detection near [111]. Another prominent feature is the ν branch which has a minimum frequency for **B** ∥ [111]. Some branches, e.g., μ and γ [Fig. 1(a)], show small splittings which could arise from extremely small corrugations in the FS or a small misalignment of the sample. The ν branch is a signature of the neck around the L point in the [111] direction and is in excellent quantitative agreement with the neck for the minority spin ($\downarrow$) of band 28. Although three sheets of the FS are predicted to have necks along $\langle 111 \rangle$ (orbits $L_{28,\downarrow}$, $L_{28,\uparrow}$, $L_{29,\downarrow}$) only one necklike branch is observed. The most likely reason is that the higher masses of the $L_{28,\uparrow}$ and $L_{29,\downarrow}$ orbits (see Table I) make the signals too weak to be resolved.

The topology of sheet 28 ($\downarrow$ and $\uparrow$ spin) is reminiscent of the FS of Cu [14]. Thus, we expect to see the other orbits seen in Cu. The δ and ϵ orbits near **B** ∥ [110] ($X_{28,\uparrow}$ and $X_{28,\downarrow}$) correspond to the "dog bone" in Cu. We identify the π and ρ branches as the $W_{28,\downarrow}$ and $W_{28,\uparrow}$ calculated orbits and as the "four-cornered rosette" orbits in Cu for fields **B** ∥ [001] [14]. These orbits connect the [111] necks in neighboring Brillouin zones and are shown in Fig. 2(a). The low-frequency ξ branch appears to be due to the $W_{27,\downarrow}$. Finally, the σ branch appears to be due to either the rosette-type orbit $W_{29,\uparrow}$ or an extension of the $X_{27,\uparrow}$ branch to [001] which may occur with a small energy shift of band 27. Our calculation overestimates the size of the dog bone and "rosette" orbits on sheets 28 and 29. We note that because all these orbits are related to the necks, both frequencies would be decreased if these bands were lowered relative to E_F or if the necks opened out more rapidly along [111] than the calculation predicts.

Comparison of the measured and calculated cyclotron masses shows that the quasiparticle mass enhancements $m^*/m_b = 1 + \lambda$ are in the range of about 2–5 for $B = 9.2$ T. The linear term of the specific heat γ shows a strong field dependence, $\gamma = 35$ mJ mol^{-1} K^{-2} for $B = 9.2$ T and 47 mJ mol^{-1} K^{-2} for $B = 0$ [15], thus we expect m^* to be field dependent. Comparing the measured γ for $B = 9.2$ T with $\gamma_{\text{calc}} = (\pi^2/3)k_B^2 N_{\text{tot}}(E_F) = 9.6$ mJ mol^{-1} K^{-2} [16] we find an average mass enhancement $m^*/m_b = 3.7$ which is in the center of the range observed by dHvA. If we make the same calculation for $B = 0$, we find $m^*/m_b = 4.9$. To our knowledge, no other alloy of d-band metals shows a mass enhancement close to these. Palladium which is often taken as an example of a system with strong spin fluctuations has an enhancement of about two.

Table II summarizes the important parameters for some FS orbits in $ZrZn_2$. The measured Fermi velocity and cyclotron mass include the effects of electron correlations. The quasiparticle lifetime and mean-free path, l, are determined from the Dingle factor R_D. It is interesting to note that $l \approx 1500$–2800 Å is considerably larger than the superconducting coherence length $\xi \approx 270$ Å in this sample allowing unconventional superconductive pairing [6].

It is interesting to compare the properties of $ZrZn_2$ with other d-band ferromagnets. Figure 2(b) shows the

TABLE II. Selected measured (calculated) Fermi surface parameters for $ZrZn_2$ [17].

Branch (orbit)	$\alpha(\Gamma_{30,\downarrow})$	$\beta(\Gamma_{30,\uparrow})$	$\gamma(X_{27,\downarrow})$	$\epsilon(K_{28,\uparrow})$
F (kT)	1.42(1.19)	1.60(1.33)	1.81(1.38)	4.77(5.54)
$\langle k_{F\perp}\rangle$ (Å^{-1})	0.21(0.19)	0.22(0.20)	0.23(0.20)	0.38(0.41)
m^*, m_b (m_e)	0.82(0.24)	0.95(0.26)	1.27(−0.51)	3.9(−1.53)
v_F (Mms^{-1})	0.30(0.92)	0.27(0.90)	0.21(0.45)	0.11(0.31)
$\tau(ps)$	0.28	0.31	0.32	
l (Å)	2580	2750	1500	

paramagnetic DOS for $ZrZn_2$. The Fermi level, E_F, lies in a region where the DOS is large due to the 4d Zr band. Also shown in Fig. 2(b) are the relative shifts of E_F for both spins in the ferromagnetic state. The small exchange splitting ($\Delta \approx 70$ meV) of $ZrZn_2$ means that the Fermi levels for both spins remain in the high DOS region giving $ZrZn_2$ its unusually large DOS in the ferromagnetic state in contrast with Fe and Ni (Table III). In the "stronger" ferromagnets, $N_{\rm tot}(\epsilon_F)$ is considerably less in part due to the larger exchange splitting moving E_F for one of the spin out of the d band. A high DOS at the Fermi energy generally favors superconductivity so this may be a key factor in understanding the superconductivity in this material.

In summary, our angle-resolved dHvA study shows that an *ab initio* LSDA calculation provides a good description of the electronic structure near E_F, allowing its use to further understand quantitatively the magnetic and superconducting properties of $ZrZn_2$. We find that $ZrZn_2$ has a very large DOS at E_F compared to other d-band ferromagnets both because of the presence of several large sheets of FS and because the Fermi levels for both majority and minority spins lie in the Zr d band in the ferromagnetic state. Further, the fermion quasiparticles are strongly enhanced with an average mass enhancement of about 4.9. This value is large for materials containing only d-band metallic elements and comparable with that found in the oxide system Sr_2RuO_4 [19]. The presence of the high quasiparticle density of states naturally explains the very large electronic heat capacity observed in $ZrZn_2$ and also the unsaturated magnetic moment (or large intrinsic magnetic susceptibility) in the ferromagnetic state. Finally, the high quasiparticle DOS will favor superconductivity.

TABLE III. Magnetic moment, μ, exchange splitting, Δ, DOS at E_F compared between $ZrZn_2$, Fe, and Ni [18].

	Fe	Ni	$ZrZn_2$
$\mu = n_\uparrow - n_\downarrow$ (μ_B/f.u.)	2.12	0.56	0.16
Δ (eV)	2.2	0.6	0.07
$N_\uparrow(E_F)$ (eV^{-1} f.u.$^{-1}$ spin^{-1})	0.83	0.17	2.39
$N_\downarrow(E_F)$ (eV^{-1} f.u.$^{-1}$ spin^{-1})	0.25	1.50	1.80
$N_{\rm tot}(E_F)$ (eV^{-1} f.u.$^{-1}$)	1.08	1.67	4.19

We are grateful to N. R. Bernhoeft, B. L. Györffy, G. G. Lonzarich, Zs. Major, C. Pfleiderer, and J. B. Staunton for their help with this work. Support from the EPSRC, the Swiss National Science Foundation (G. S.), and the Royal Society (P. J. M. and S. B. D.) is also acknowledged.

[1] S. S. Saxena *et al.*, Nature (London) **406**, 587 (2000).
[2] C. Pfleiderer *et al.*, Nature (London) **412**, 58 (2001).
[3] D. Aoki *et al.*, Nature (London) **413**, 613 (2001).
[4] K. Shimizu *et al.*, Nature (London) **412**, 316 (2001).
[5] N. F. Berk and J. R. Schrieffer, Phys. Rev. Lett. **17**, 433 (1966); D. Fay and J. Appel, Phys. Rev. B **22**, 3173 (1980).
[6] A. P. Mackenzie *et al.*, Phys. Rev. Lett. **80**, 161 (1998).
[7] K. Ishida *et al.*, Nature (London) **396**, 658 (1998).
[8] D. J. Singh and I. I. Mazin, Phys. Rev. Lett. **88**, 187004 (2002).
[9] P. C. Canfield, P. L. Gammel, and D. J. Bishop, Phys. Today **51**, No. 10, 40 (1998); I. Felner *et al.*, Phys. Rev. B **55**, R3374 (1997).
[10] D. Shoenberg, *Magnetic Oscillations in Metals* (Cambridge University Press, Cambridge, 1984).
[11] P. G. Mattocks and A. E. Dixon, J. Phys. F **11**, L147 (1981); J. M. van Ruitenbeck *et al.*, J. Phys. F **12**, 2919 (1982); A. P. J. van Deursen *et al.*, J. Magn. Magn. Mater. **54–57**, 1113 (1986); I. Lo, S. Mazumdar, and P. G. Mattocks, Phys. Rev. Lett. **62**, 2555 (1989).
[12] G. Santi, S. B. Dugdale, and T. Jarlborg, Phys. Rev. Lett. **87**, 247004 (2001).
[13] R. A. de Groot, D. D. Koelling, and F. M. Mueller, J. Phys. F **10**, L235 (1980); T. Jarlborg, A. J. Freeman, and D. D. Koelling, J. Magn. Magn. Mater. **23**, 291 (1981).
[14] A. B. Pippard, Philos. Trans. R. Soc. London, Ser. A **250**, 325 (1957); D. Schoenberg, *ibid.* **255**, 85 (1962); A. S. Joseph *et al.*, Phys. Rev. **148**, 569 (1966). See also Ref. [10].
[15] C. Pfleiderer *et al.*, J. Magn. Magn. Mater. **226**, 258 (2001).
[16] We neglect the field dependence of $N_{\rm tot}(E_F)$, which we estimate to be about 10% for $B \approx 10$ T.
[17] We calculate the FS parameters as follows: $\langle k_F\rangle = \sqrt{A/\pi}$, $v_F = \hbar\langle k_F\rangle/m^*$, and $l = v_F\tau = \hbar\langle k_F\rangle\tau/m_b$.
[18] J. Callaway and C. S. Wang, Phys. Rev. B **16**, 2095 (1977); C. S. Wang and J. Callaway, *ibid.* **15**, 298 (1977).
[19] A. P. Mackenzie *et al.*, Phys. Rev. Lett. **76**, 3786 (1996).